AN INVESTIGATION OF THE SINTERING KINETICS OF LEAD POWDERS

Final Technical Report

August, 1977

Patrick K. Higgins
Graduate Research Assistant

Zuhair A. Munir
Principal Investigator

ABSTRACT

An analysis of the parameters involved in the sintering of lead powders under vacuum has been made. Sintering was accomplished at temperatures between 250° and 280°C. Evaluation of surface area reduction data results in values of the mechanism exponent N between 5.3 and 6.7. Lack of shrinkage and the low vapor pressure of lead at the experimental temperatures lead to the conclusion that surface diffusion is the rate-controlling sintering mechanism. However, comparison of the experimentally measured activation energy, 170 KJ/mol (40.7 Kcal/mol), to that reported in the literature for surface self-diffusion of lead showed a significant discrepancy. Effects of pore isolation and surface oxide layers are proposed as possible explanations for this discrepancy as well as the deviation in the N values from those obtained theoretically. An attempt to isolate the effect of the oxide layer was made by sintering lead in a hydrogen atmosphere. Under these conditions, sintering is accompanied by shrinkage, thus indicating the presence of a bulk-transport process. A mechanism exponent corresponding to viscous flow sintering was obtained. Furthermore, the calculated activation energy for this process was in good agreement with that reported for creep in lead.

Acknowledgments

We are grateful to Dr. Ralph Condit whose aid and advice have added immeasurably to the scope of this investigation. The assistance of Charles Siettevold of LLL and Bill Weigt and Don Barnum of UCD is gratefully acknowledged. We are also appreciative of the helpful discussions with Drs. Clarence Hoenig and Charles Folkers.

This work was supported by a grant from the Lawrence Livermore Laboratory under Intramural Purchase Order 4879803.

TABLE OF CONTENTS

LIST OF FIGURES

LIST OF TABLES

INTRODUCTION

The investigation of the parameters involved in the sintering of lead powder compacts is prompted by the desire to use oxidized lead powder as a first wall tritium diffusion barrier for nuclear reactors. In order to completely understand the diffusion mechanisms involved in the sintering of the oxidized lead it is desirable to first gain knowledge of those mechanisms which control the sintering of the substrate material, lead. A literature search showed no prior publications on the sintering of lead, thus an experimental determination of the kinetics of sintering of this metal was initiated.

The first investigations into sintering as a forming process coincided with the growing use of sintered tungsten by the incandescent light industry in the 1920's. Until the work of Sauerwald[1] little was known of the mechanisms involved in the process. Sintering may be defined as the heat treatment of a system of particles or a porous body in which in individual cases some or all of the properties of the system change, and in every case the reduction of free energy is the driving force. In the compact this free energy may be found in the form of excess surface energy, an energy gradient due to surface curvature, and excess lattice energy due to vacancies, dislocations, and internal stresses.[2] The reduction of free energy is accomplished by the creation and growth of necks between particles within the compact through movement of matter on the atomic level.

Several variables affect the kinetics of the sintering process. These are temperature, particle size, initial compact density, composition, and sintering time. As the isothermal sintering time is allowed to increase the rate of neck growth diminishes due to a diminishing thermodynamic potential gradient between individual particles. The first effort to model

this process on a theoretical basis was made by Frenkel[3] in 1945 and by Kuczynski[4,9] in 1949. Kuczynski's major contribution to the understanding of sintering was his recognition of a multi-mechanism process where one or more transport paths can be operative.

Kuczynski proposed the following relationship to describe the sintering of spherical powders:

$$(x/a)^N = Bt \qquad (1)$$

where x/a is the ratio of the neck radius x to the particle radius a as shown in Figure 1, N is an exponent characteristic of the particular mechanism, t is the isothermal sintering time, and B is a material parameter encompassing surface energy, atomic spacing, diffusivity, particle size, and temperature. Specific definitions of B are listed in Table 1.

Since introduction of the Kuczynski equation five independent sintering mechanisms have been identified: surface diffusion, evaporation-condensation, viscous flow, grain boundary diffusion, and volume diffusion. Of these the first two do not result in shrinkage during sintering and are categorized as surface-transport mechanisms while the remaining three, which result in shrinkage during sintering, are categorized as bulk-transport mechanisms. Table 1 also lists the various values obtained for the parameters within the Kuczynski equation. Although other value for N and B have been obtained those listed in Table 1 are the most widely accepted.

Application of Kuczynski's model to experimental data has proven its usefullness in the sintering process. A log-log plot of x/a versus t results in a straight line whose slope is the characteristic exponent N and intercept is the constant B. Assuming mechanisms to operate singularly, Herring[6] stated that the time necessary to achieve similiar degrees of sintering varies with respect to mechanism and proposed that

$$t_1 = \lambda^{\omega} t_2 \qquad (2)$$

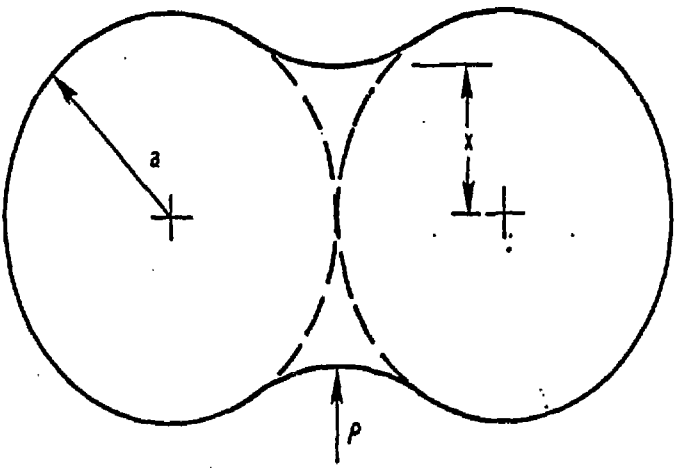

a) Surface-transport: no shrinkage

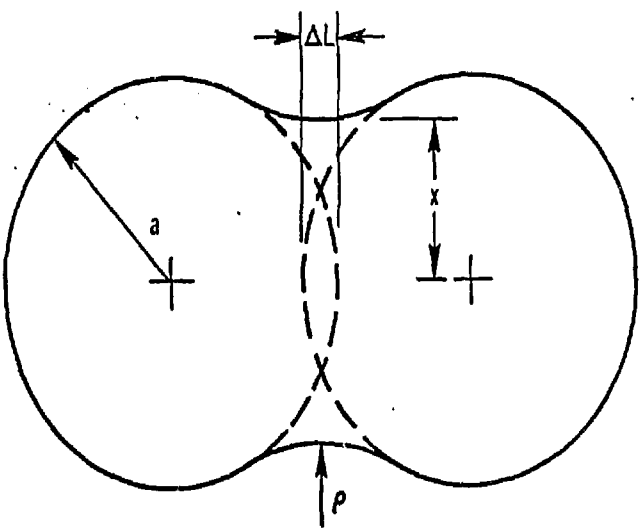

b) Bulk-transport: with shrinkage

Figure 1 Geometric sintering models employed in Kuczynski's equation.

Table 1 Materials parameters in sintering equations.

Mechanism	B	N	ω	Ref.
Surface Diffusion	$\frac{56\,\gamma\,\delta^4\,D_s}{a^4\,kT}$	7	4	4
Evaporation-Condensation	$\frac{3\,\pi\,\gamma\,P_o}{a^2\,d^2}\left[\left(\frac{M}{kT}\right)^3\frac{1}{2\pi}\right]^{.5}$	3	2	8
Viscous Flow	$\frac{3\gamma}{2\,a\,\eta}$	2	1	9,4
Grain Boundary Diffusion	$\frac{24\,\gamma\,\delta^4\,D_{GB}}{\pi\,a^4\,kT}$	6	4	10
	$\frac{480\,\gamma\,\delta^3\,D_{GB}}{a^4\,kT}$	6	4	11
Volume Diffusion	$\frac{80\,\gamma\,\delta^3\,D_V}{a^3\,kT}$	5	3	8
	$\frac{40\,\gamma\,\delta^3\,D_V}{a^3\,kT}$	5	3	4

γ = surface energy, δ = atomic spacing, a = particle size, k = Boltzmann's constant, T = absolute temperature, η = viscosity, M = atomic mass, P_o = equilibrium vapor pressure, d = density, D_s = surface diffusion coefficient, D_{GB} = grain boundary diffusion coefficient, and D_V = volume diffusion coefficient.

where t_1 and t_2 are sintering times at which identical degrees of sintering are achieved, λ is the ratio of the particle radii a_1 and a_2, and ω is a mechanism characteristic constant. Values of ω are also given in Table 1.

Recent advances in the field of sintering have both enhanced our understanding of the mechanisms and improved the proposed sintering models thus making interpretation of experimental data less tedious. Inherent to the Kuczynski model is the need to accurately measure the change in neck dimensions as sintering progresses. Until recently, measurements were made using optical microscopy. Besides being tedious this method requires a sufficiently large number of samples to give statistical validity to the measurements. Therefore the need for an accurate method of determining the degree of sintering has received much attention.

Ibrahim and Jellinek[7] proposed that the change in surface area of a compact and neck growth can be related by the following:

$$\Delta S/S_0 = k_1(x/a)^2 + k_2(x/a)^3 \qquad (3)$$

where ΔS is the change in surface area relative to an initial value S_0, and k_1 and k_2 are constants. By use of mathematical models German and Munir[8] showed that the surface area reduction has the following dependence on neck size:

$$\Delta S/S_0 = K(x/a)^m \qquad (4)$$

where K and m are both coordination number and mechanism-dependent constants. Figures 2 and 3 show the variation with coordination number of both K and m, respectively.[8] Finally by combining Equation (4) with Equation (1) one obtains:

$$\Delta S/S_0 = K(Bt)^{m/N} \qquad (5)$$

A log-log plot of $\Delta S/S_0$ versus t results in a straight line dependence where the slope is m/N. From the calculated values of m, Figure 3, the exponent N can be determined.

German and Munir[9,10] have also shown that the values for the constants

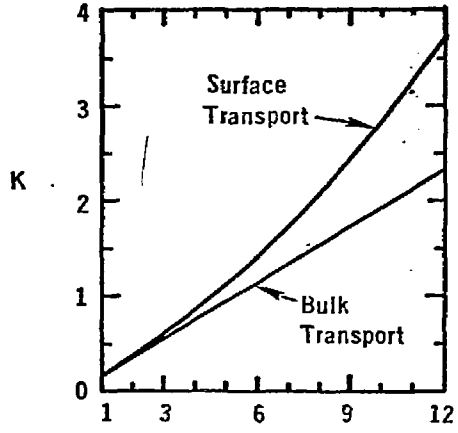

Figure 2 The variation of K with coordination number.

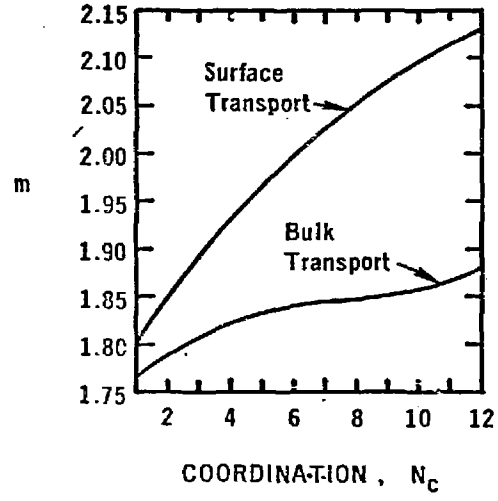

Figure 3 The variation of m with coordination number.

k_1 and k_2 in Equation (3) are

$$k_1 = 0.2278\ N_c$$
$$k_2 = 0.0215\ N_c^2 - 0.0907\ N_c \tag{6}$$

for surface-transport mechanisms and

$$k_1 = 0.2607\ N_c$$
$$k_2 = -0.0915\ N_c \tag{7}$$

for bulk-transport mechanisms. Here N_c is the coordination number of the powder compact. Thus the relationship between surface area and neck size is

$$\Delta S/S_o = 0.2278\ N_c\ (x/a)^2 + (0.0215\ N_c^2 - 0.0907\ N_c)\ (x/a)^3 \tag{8}$$

for surface-transport mechanisms and

$$\Delta S/S_o = 0.2607\ N_c\ (x/a)^2 - 0.0915\ N_c\ (x/a)^3 \tag{9}$$

for bulk-transport mechanisms. Furthermore, work by Munir, Higgins, and German[11] has shown that combination of Equation (3) and (5) results in the expression:

$$K\ (Bt)^{m/N_o} = k_1\ (x/a)^2 + k_2\ (x/a)^3 \tag{10}$$

where k_1 and k_2 take on the appropriate values for surface or bulk-transport processes. The subscript (o) for the mechanism exponent N is placed to show a non-dependence on neck size or coordination number. Thus we define

$$N = fN_o \tag{11}$$

where f is a factor containing the dependence of N on coordination number and neck size. Introducing this into equation (1) gives

$$(x/a)^{fN_o} = Bt \tag{12}$$

and by defining

$$P = k_1/K \text{ and } Q = k_2/K \tag{13}$$

and rearranging Equation (10) the following expression results:

$$f = \frac{\ln\ \left[P(x/a)^2 + Q(x/a)^3\right]}{m\ \ln(x/a)} \tag{14}$$

This expression represents the variation of the characteristic mechanism

exponent with respect to changes in particle coordination and neck growth. Variation of experimental data from the straight line log-log plot proposed by Kuczynski is thereby accounted for by differences in coordination and by the degree of growth of the neck region between particles.

In circumstances where two independent mechanisms are operating simultaneously, German and Munir[12] have shown that by taking the ratio of the rate equations for the two mechanisms it is possible to distinguish the regions of dominance of each mechanism. The equation derived is

$$\frac{(\dot{x}_1/a)}{(\dot{x}_2/a)} = K(x/a)^n \qquad (15)$$

where

$$K = \frac{B_1 N_2}{B_2 N_1} \qquad (16)$$

$\dot{x}_1$ and $\dot{x}_2$ are the rates of neck growth of the two mechanisms, and n is the difference between the two characteristic exponents, i.e. $N_2 - N_1$. Although this technique is applicable only to mechanisms which act independently of each other, it does account for neck growth and is applicable to surface-transport as well as bulk-transport mechanisms.

Many early investigators in the field of sintering assumed the driving force to be the reduction of surface area in the compact. Investigators[13,14], using this assumption, arrived at the following kinetic expression:

$$dS/dt = -kS^m \qquad (17)$$

where k and m are constants. Recently, German and Munir[15] expressed the equation in the general form

$$(\Delta S/S_o)^\gamma = Ct \qquad (18)$$

where $\Delta S = S_o - S$, S is the instantaneous surface area, S_o is the initial surface area, t is the isothermal sintering time, γ is a factor related to the mechanism by particle coordination, and C is a constant related to the

geometry, kinetics, and material properties of the compact.

Since Equation (17) only partially accounted for the results compiled through experimentation, it was postulated[15] that another driving force must become dominant at some time during the sintering process. By differentiation of Equation (18) the expression

$$dS/dt = - C/\gamma \left[S_o^{\gamma} / (\Delta S)^{\gamma-1} \right] \qquad (19)$$

is obtained. This expression is the kinetic equation for sintering when the gradient of surface curvature is the driving force. It was thus shown that the initial driving force for sintering is the gradient of surface curvature. Then as neck size increases and surface curvature gradients decrease, the driving force becomes dominated by the reduction of surface area. Data may then be plotted to determine which driving force is applicable. If the data show a linear dependence in a log-log plot of dS/dt versus $\Delta S/S_o$ then surface curvature is the dominant driving force. If the same data show a linear dependence in a log-log plot of dS/dt versus S then Equation (17) is applicable and reduction of surface area is the driving force.

One final consideration in understanding the basic models of sintering is the effect of grain growth. Considering each sphere in the compact to be a single grain then grain growth involves the growth of a neck between the two grains, followed by migration of the grain boundary, and, if allowed to continue to completion, spheroidization of the resulting particle. The migration of the grain boundary is a result of a driving force for reduction of excess grain boundary energy. Growth always occurs in a direction such that the boundary moves toward its center of curvature. As large grains grow at the expense of smaller ones the average grain size increases causing a net reduction in the overall excess surface energy. This causes a subsequent reduction in the rate of sintering due to a decrease in the driving force. Furthermore, as grain growth continues pores begin to become isolated result-

ing in a further reduction in the sintering rate. This is due to the minimization of grain boundary-pore surface contact area and if allowed to occur will result in an exceedingly slow sintering rate and thus a low final density. Since isolation of pores is a function of the sintering mechanism and rate[16], its control may be experimentally achievable.

Even though no specific reference is made in the literature to previous work on the sintering of lead, several authors have examined this process for tin. An analysis of the sintering of tin may show similarities in their kinetic behavior due to the similarity of their properties. Both metals have low melting points (232°C for tin and 327°C for lead), both have 2,4 valence states and are group IV metals, and both react rapidly with oxygen at room temperature to form stable tetragonal monoxides[17]. Furthermore, both of these metals are media for fast diffusion of dissolved Au, Ag, etc., and are thus unlike most other metals. As early as 1921 Smith[18] stated that tin, as well as manganese, did not sinter even at temperatures approaching their melting points. More recently, Smart and Ellwood[19] attributed this behavior to the effect of an oxide layer, and concluded that the role of the sintering atmosphere is important especially with low melting point materials. Moreover, the work of Smart and Ellwood showed that removal of the oxide layer allowed sintering to occur at a rate more in line with expected behavior.

In view of these considerations and in accordance with the objectives stated earlier, an investigation of the kinetics of sintering of powder compacts of lead was undertaken.

EXPERIMENTAL PROCEDURE

A) Sample Preparation

To evaluate the kinetic parameters of Kuczynski's equation spherical lead powder within the range of 10 to 20 μm was used. The lead was 99.9% pure with typical impurities listed in Table 2. It is difficult to ascertain the affect of impurities at levels in the parts per million range on sintering experiments.

Specimens were first weighed into approximately two-gram samples. A special graphite die was constructed employing a double piston action to apply a static load across a 0.64 cm (0.25 inch) diameter piston, Figure 4. A Tinius-Olsen press was used to load the die to a pressure of 17.5 MPa (2550 psi). This pressure results in a pellet with a 0.65 cm (0.257 inch) diameter, a height of approximately 0.76 cm (0.300 inch), and a density of about 68% of the theoretical value for lead (11.36 gm/cm^3). Specimens were then divided into groups of four for use in individual tests. The groups were then placed into an argon filled dessicator until their use.

B) Furnace

The system is a bell-jar vacuum apparatus with a Kinney mechanical pump and a Varian NRC/NHS-6 six inch diffusion pump with a 1500 l/sec pumping speed (Figures 5 and 6).

The bell-jar contains a specially designed horizontal tube furnace, Figure 7, with a maximum temperature capability of 1500°K. The furnace consists of a 2.54 cm (1.0 inch) molybdenum core enclosed at 0.64 cm (0.25 inch) intervals by four molybdenum heat shields. The shield separation is maintained by lavite insulators at the furnace ends and lavite rings at the center. Current to the furnace is carried by a 0.95 cm (0.375 inch) copper tube making electrical contact with the molybdenum core via brass disks which are silver

Table 2 Typical impurity concentrations in the lead powders.

Element	ppm *	Element	ppm *
Ga	600	Fe	25
Bi	200	Ti	10
Sn	70	Ca	9
Al	50	Mg	2
Cu	25	Ag	1
		Total	992 ppm

Tested but not detected:

B, Ba, Be, Co, Cr, Mn, Mo, Na, Nb, Ni, Sb, Sr, V, Zn, Zr

* ppm = part per million

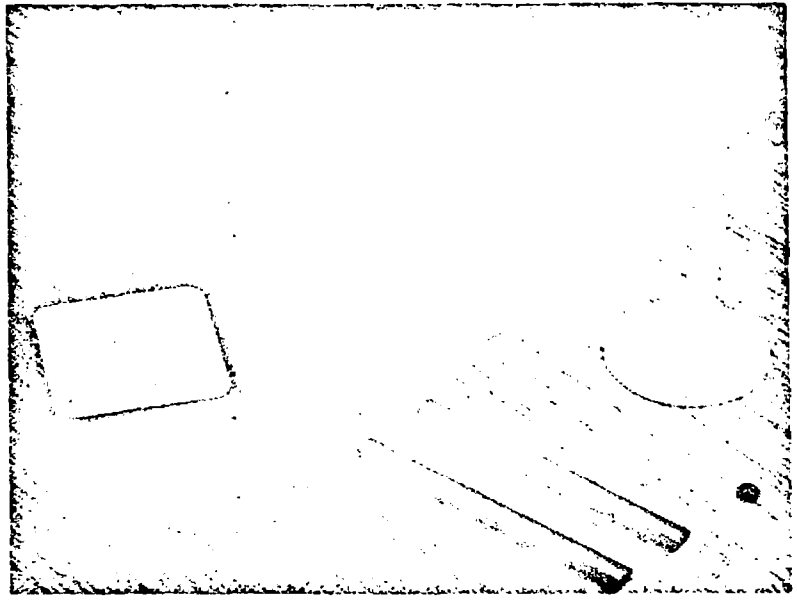

Figure 4 Specimen die with dual piston action.

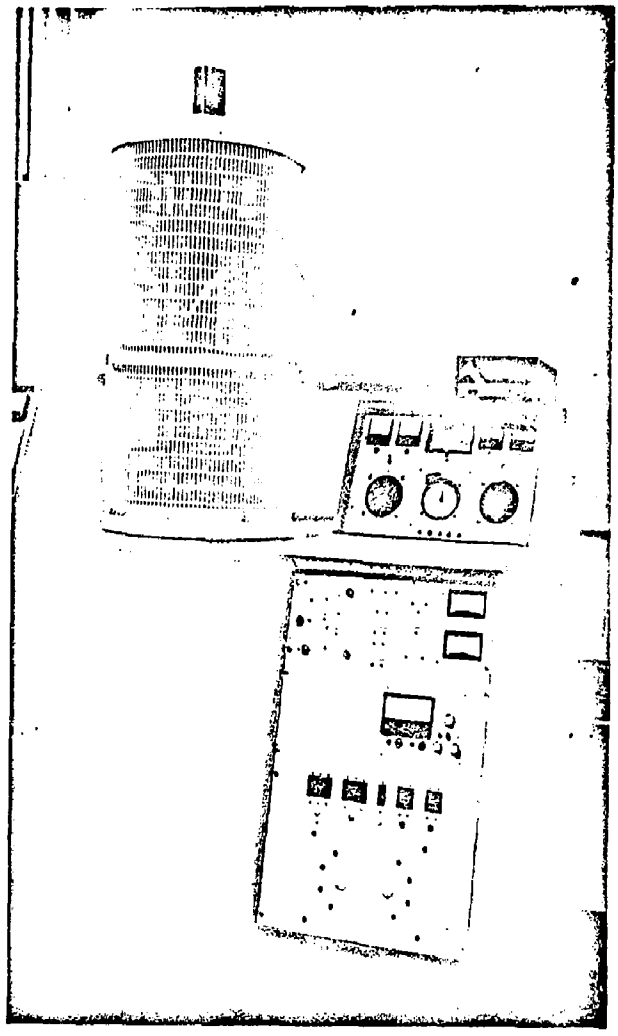

Figure 5 The bell-jar vacuum system.

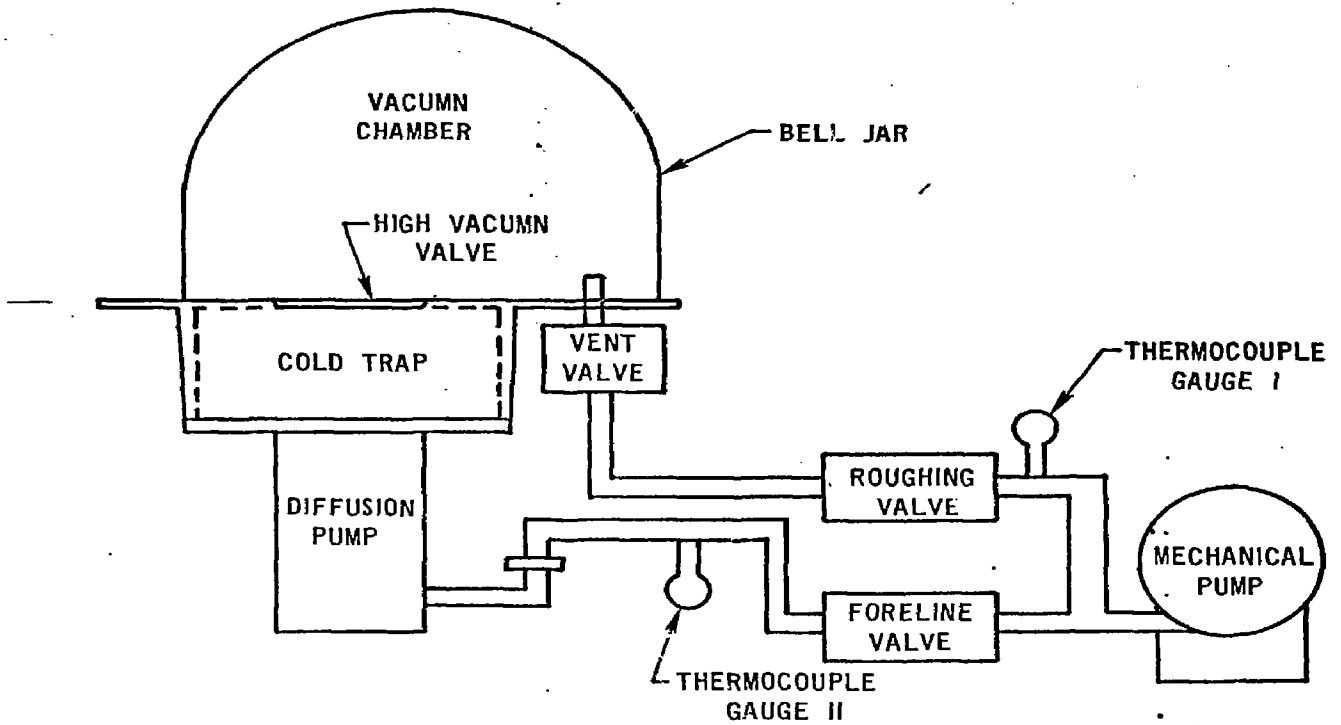

Figure 6 Schematic diagram of the bell-jar vacuum system.

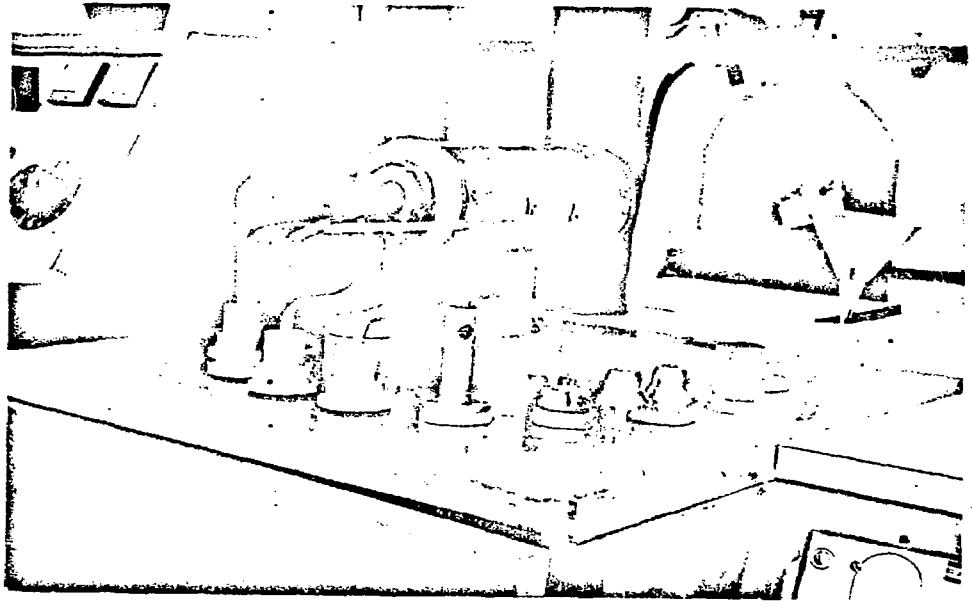

Figure 7 A close-up of the horizontal sintering tube furnace.

soldered to the core. Cooling water flowing through the copper tubing maintained both ends of the furnace at temperatures close to ambient. Brass plugs placed at each end of the molybdenum core increased the length of the constant-temperature region within the furnace. A graphite "dee" 1.27 cm (0.50 inch) in radius gave a flat surface on which specimens were placed. Temperature was measured by means of a Chromel-Alumel thermocouple which was inserted through the "dee" at the center point of the furnace.

The temperature was monitored by two separate Chromel-Alumel thermocouple circuits, Figure 8. The first thermocouple monitors the furnace temperature and by implementation of an L.F.E. Electronics Optical Meter Relay Time Proportioning Module Model API909B regulates the furnace power. This module has a capability of locking to and controlling temperature to within $\pm 0.5^{o}$K. The second thermocouple was used to read the furnace temperature by the output of a Dana 3800 Digital Multimeter Voltmeter.

Lead pellets were placed on the graphite "dee" within 0.32 cm (0.125 inch) of the monitoring thermocouples. The system was then evacuated to a minimum vacuum of 0.13 μPa (10^{-7} torr). The extent of vacuum was continuously measured by a Consolidated Vacuum Corporation IG-101K 2.54 cm (1.0 inch) Kovar tubulation vacuum ion gauge. This gauge was monitored by a Veeco Model RG830 Ionization Gauge Control. A heating rate of Approximately 50^{o}K/min was utilized.

C) The B.E.T. Surface Area-Pore Volume Analyzer

The apparatus described here was at the Lawrence Livermore Laboratory (LLL) where the surface area measurements were made. The apparatus consists of a vacuum system, a pressure transducer, temperature monitors, sample chambers, and an interconnecting manifold system. All piping was of Monel 400, see Figure 9.

The vacuum system was comprised of a cold trap, a diffusion pump, and a forepump. The diffusion pump has a pumping speed of 11 l/sec with a limiting

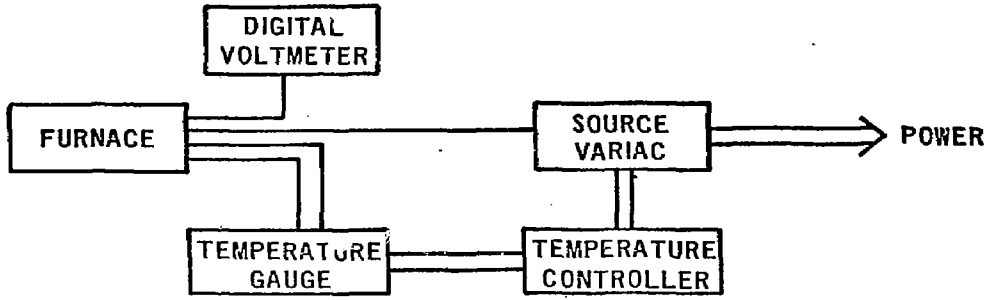

Figure 8 Schematic diagram of the temperature monitoring and control system.

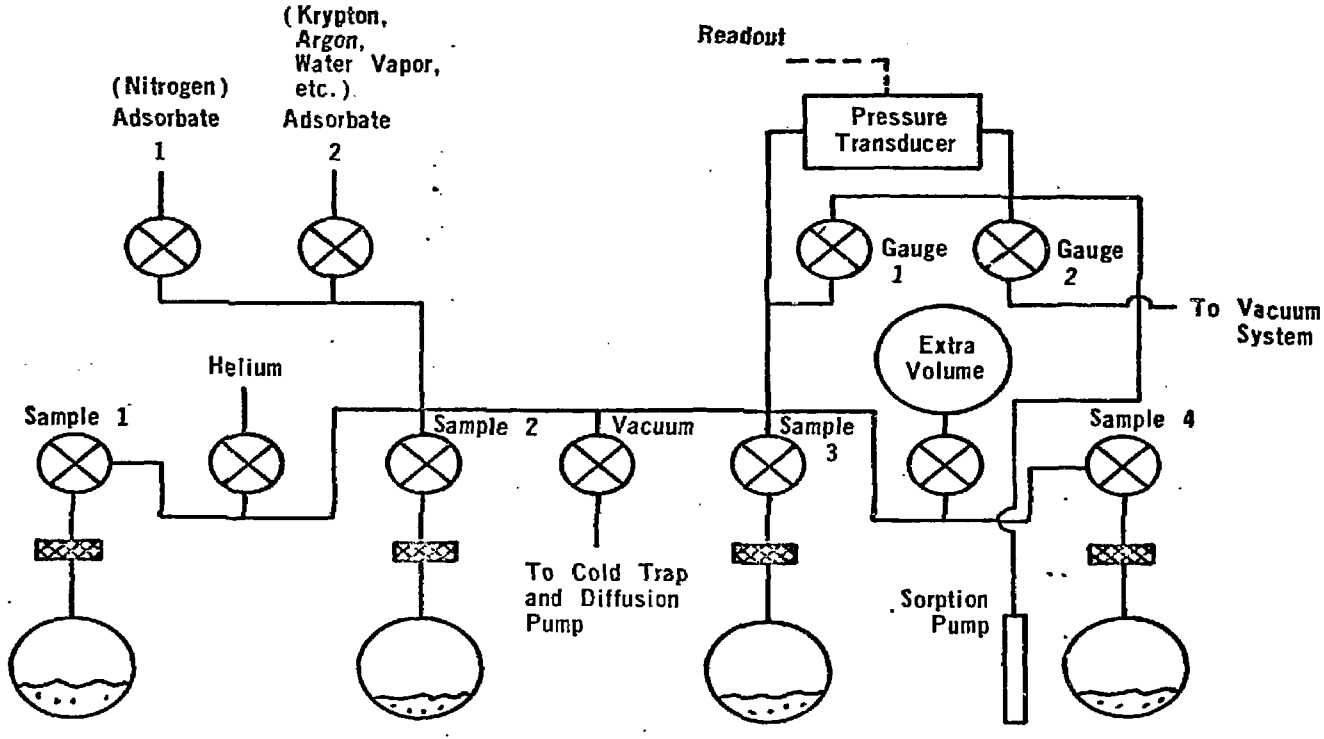

Figure 9 Schematic diagram of the B.E.T. surface area measurement apparatus (LLL facility).

forepressure of 13 Pa (0.1 torr). The forepump has an ultimate vacuum of 1.33 cPa (10^{-4} torr) giving the complete apparatus an ultimate vacuum of 13.3 mPa (10^{-6} torr). Pressure is measured by a null point detector[20], Figure 9. It is detected by means of a specially designed electronic manometer using dual pressure transducer. Temperature in the liquid nitrogen regime were measured by thermister probes to within $\pm 0.1^{\circ}K$.

D) Experimental Methods

Three sintering temperatures were selected with four sintering times per temperature. Four specimens were sintered at each time. The selected temperatures were 250, 268°, and 280°C which correspond to 0.76, 0.81, and 0.86, respectively, of the melting point of pure lead. The sintering times were 30, 60, 120, and 300 minutes. As-pressed samples (zero sintering time) were used as a reference in determining change in surface area as a function of time.

After the completion of each individual experiment the system was cooled by the introduction of argon gas. Each group was then marked and the surface area measured by the B.E.T. method, see Appendix 1. One specimen from each group was used to take hardness reading and to provide microstructural information.

RESULTS

Scanning electron micrographs (SEM) of the sintered and unsintered lead powders are shown in Figures 10, 11, and 12. Micrographs of unsintered powder are shown in Figure 10 while a time dependent sequence of sintered powders is shown in Figures 11 and 12. The micrographs of Figure 11 are of powders sintered at 250°C in vacuum at a magnification of 7500X. Time dependent growth of the neck region between particles is evident as sintering time increases. Figure 12 shows a similiar sequence of micrographs for powders sintered at 280°C. These micrographs were taken at a magnification of 7200X. Again the increase in neck growth with sintering time is evident. The difference in magnification makes a direct comparison of the two figures difficult, however, careful observation of the two figures shows a noticeable difference in the neck growth rate of pellets sintered at 250°C and those sintered at 280°C. This temperature dependence of the growth rate of the neck between particles is encompassed within the constant B of Kuczynski's equation.

The change in the Vicker's hardness (136° Diamond Pyramid) of the sintered lead pellets with the isothermal sintering time is shown in Figure 13. Plotted on a log-log scale the data of Table 3, Appendix 2, give a straight line relationship of the type

$$\Delta H/H_0 = At^b \qquad (20)$$

where ΔH is the change in hardness of the sintered pellets normalized to an initial value H_0, t is the isothermal sintering time, and A and b are material dependent constants. The value of A and b have not been analytically related to the typical sintering parameters presented in an earlier section, but could be used as an indication of sintering since b is related indirectly to the N value in Kuczynski's equation.

Measurement of the pellets height and density showed no significant

(a)

(b)

Figure 10 Unsintered lead powders (SEM, 7200X)

Figure 11(a) Vacuum sintered lead powders (60 min, 250°C)(SEM, 7500X)

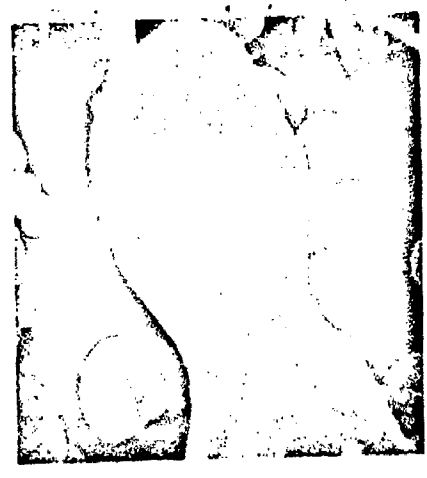

Figure 11(b) Vacuum sintered lead powders (120 min, 250°C)(SEM, 7500X)

Figure 11(c) Vacuum sintered lead powders (300 min, 250°C)(SEM, 7500X)

Figure 12(a) Vacuum sintered lead powders (30 min, 280°C)(SEM, 7200X).

Figure 12(b) Vacuum sintered lead powders (60 min, 280°C)(SEM, 7200X).

Figure 12(c) Vacuum sintered lead powders (120 min, 280°C)(SEM, 7200X).

Figure 12(d) Vacuum sintered lead powders (300 min, 280°C)(SEM, 7200X).

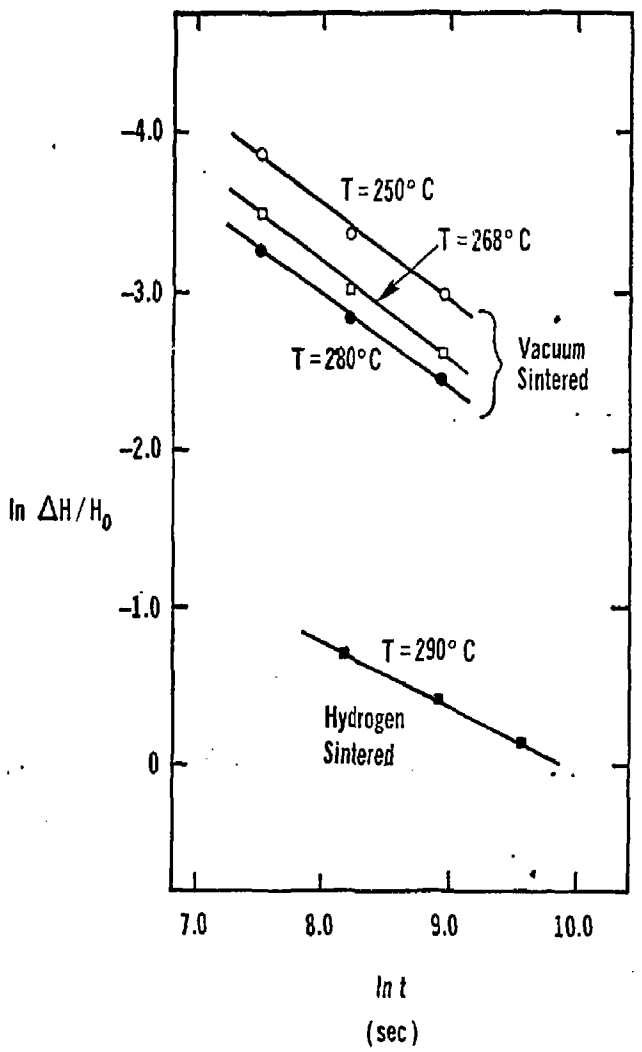

Figure 13 Variation of hardness with sintering time for lead powders sintered in vacuum and hydrogen.

Table 3 Hardness data for vacuum sintered lead pellets.

Temperature (°C)	Time (sec)	Vicker's Hardness
250	As Is	28.5
	1800	29.1
	3600	29.5
	7200	29.9
	18000	30.9
268	As Is	30.0
	1800	30.9
	3600	31.5
	7200	32.0
	18000	32.6
280	As Is	30.0
	1800	31.0
	3600	31.7
	7200	32.3
	18000	32.8

change is these parameters with sintering. Typical variation in height was of the order of 0.37% and was not a function of sintering temperature or time (Appendix 2). This variation in pellet height corresponds to a density change of 0.37%. These observations lead to the conclusion that a surface-transport mechanism is operative and therefore a B.E.T. surface area analysis was made. Results of this analysis are shown in Table 4 and Appendix 2 and are plotted in Figure 14 with a confidence limit of 91% or better. Measurement of the surface area reduction, $\Delta S/S_0$, was complicated by several factors. The low surface area per unit volume of the lead powder, typically 0.20 m^2/gm, made measurement of a change in surface area difficult. In such cases Krypton gas is usually used as the adsorbate. Additional difficulties arise from the relatively high density of the pellets and the possible concomitant pore isolation. This problem will be discussed further at a later point. However, fitting these surface area reduction data to the model of German and Munir (Equation 5) results in slopes of 0.348, 0.383, and 0.300 for the sintering temperatures of 250°, 268°, and 280°C, respectively. For m equal to 2.02, which corresponds to a particle coordination of seven, these slopes correspond to N values of 5.8, 5.3, and 6.7 for the respective temperatures. It should be pointed out here that the generally accepted value for a surface diffusion mechanism is N = 7. Although some of the experimentally determined N values are significantly different from 7 lack of shrinkage and the relatively low vapor pressure of lead point to surface diffusion as the dominating mechanism.

A plot of $\Delta S/S_0$ versus inverse sintering temperature at a constant value of the sintering time, 60 min, is shown in Figure 15. When plotted on a semi-log scale the slope of the line is related to the activation energy of the process by

$$L = \frac{Q}{R}\gamma \qquad (21)$$

where L is the slope, R is the gas constant, γ is the inverse slope, m/N, as

Table 4 Surface area reduction data for vacuum sintered lead powders.

Temperature (°C)	Time (sec)	$\Delta S/S_o$
250	1800	0.0702
	3600	0.0855
	7200	0.1256
	18000	0.1506
268	1800	0.1005
	3600	------
	7200	0.2060
	18000	0.2360
280	1800	0.1359
	3600	0.1807
	7200	0.2163
	18000	0.2865

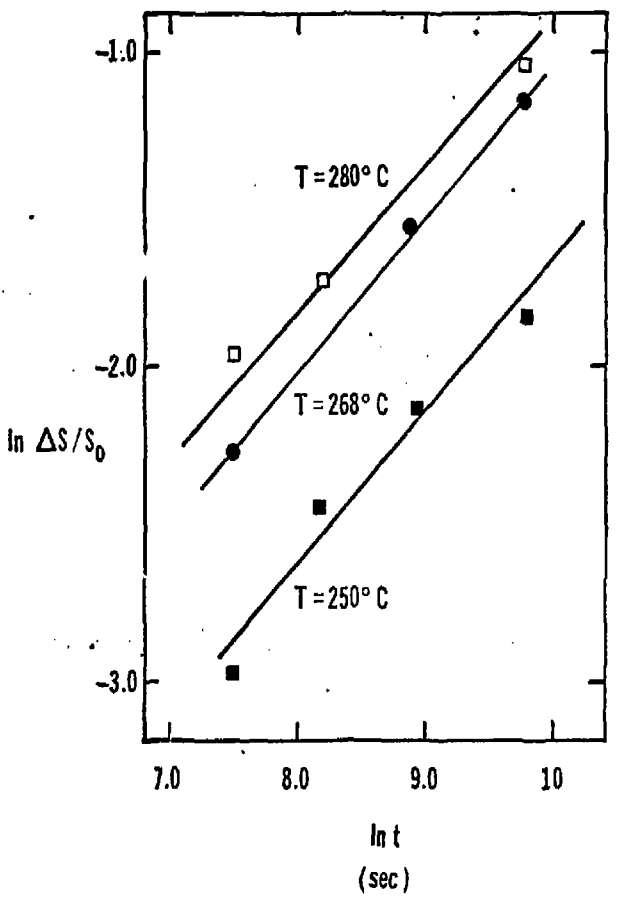

Figure 14 The variation of surface area with sintering time for vacuum sintered lead powders.

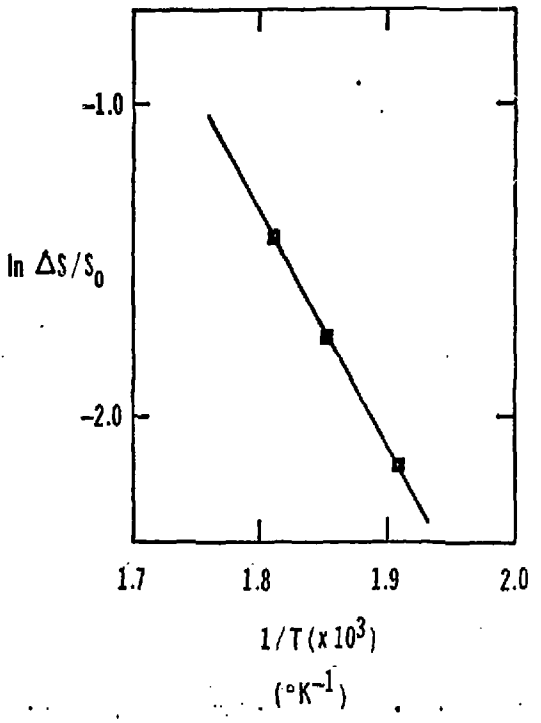

Figure 15 The temperature dependence of surface area reduction for vacuum sintered lead powders (t = 60 min).

defined by Equation 5, and Q is the activation energy of the process. The experimentally obtained value for the activation energy of the lead compacts is 170 kJ/mol (40.7 Kcal/mol). These data fit the plot with a confidence limit of 99.8%.

The effect of an oxide layer is a source of experimental difficulty and concern. In order to ascertain the role played by a stable oxide layer in the kinetics of sintering lead a number of pellets were sintered in hydrogen. Sintering under these conditions will ensure the reduction of the accessible oxide layer surrounding the lead particles. No hydrides of lead are stable at the temperatures used in this study. Preliminary results of these determinations are given in Table 5 and Appendix 2 and presented in Figures 16 through 19. In this case, and in contrast to the previous experiments which were conducted in vacuum, the powder compacts exhibited shrinkage. The data shown in Figure 16 are plotted as a time function of $\Delta L/L_o$, $\Delta d/d_o$, and $\Delta\rho/\rho_o$ where L is the length , d is the diameter, and ρ is the density of the pellet. If lines are imposed through the points of Figure 16 the resultant slopes do not give a singular value which indicates a non-uniformity or directionality of the shrinkage. However, the values of N obtained are 1.8, 2.4, and 2.6 for the axial shrinkage, radial shrinkage, and relative densification, respectively. Such values of N correspond to the viscous flow mechanism (i.e. N = 2). Hardness tests made on the pellets sintered in hydrogen at 290°C are shown in Figure 13. The slope, b of equation 20, is significantly different from that for the vacuum sintered pellets, indicating a change in the sintering mechanism and implying that the affect of the surface oxide layer is significant.

Scanning electron micrographs of lead pellets sintered in hydrogen are shown in Figure 17. Figures 17a through 17d show micrographs of pellets sintered at 270°, 280°, 290°, and 300°C, respectively. All pellets were sintered in hydrogen for one hour. A significant change in mechanism appears

Table 5 Shrinkage analysis of hydrogen sintered lead pellets.

Temperature (°C)	Time (hr)	$\Delta H/H_o$	$\Delta L/L_o$	$\Delta d/d_o$	$\Delta \rho/\rho_o$
290	1	0.4732	0.0092	0.0145	0.0350
290	2	0.6429	0.0242	0.0664	0.1777
290	4	0.8393	0.0331	0.0776	0.2076
270	1	0.3679			
280	1	0.3839			
300	1	0.5626			

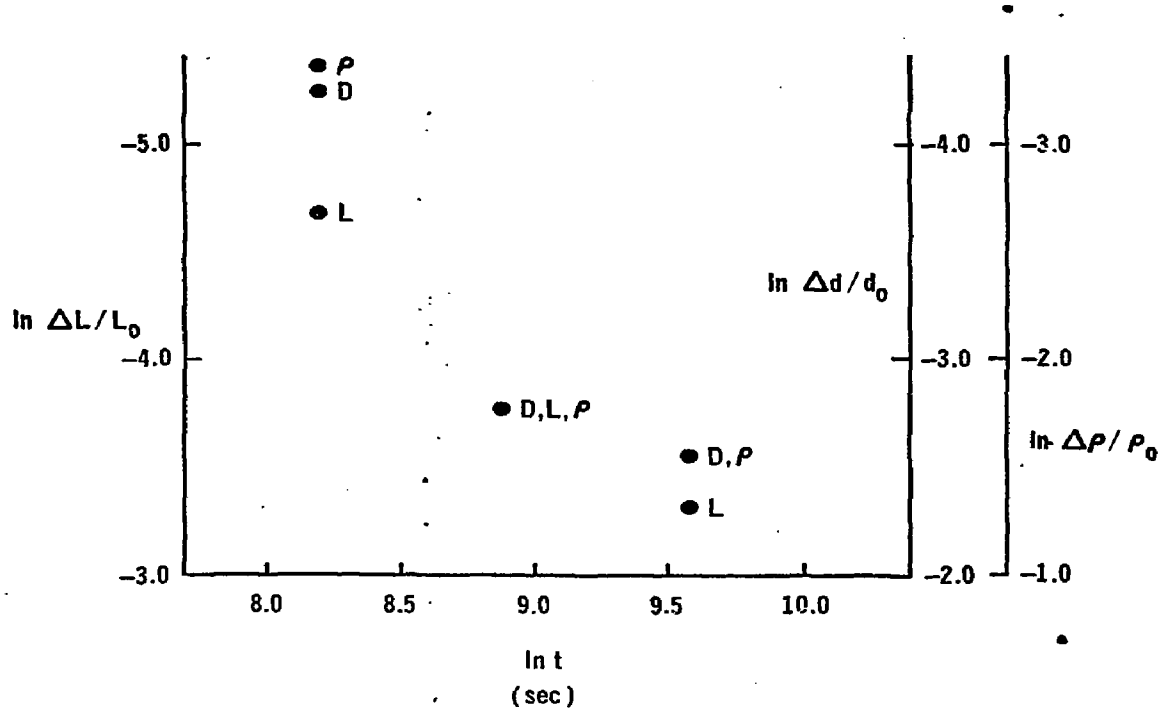

Figure 16 Variation of pellet height, diameter, and density of lead powders sintered in hydrogen (290°C).

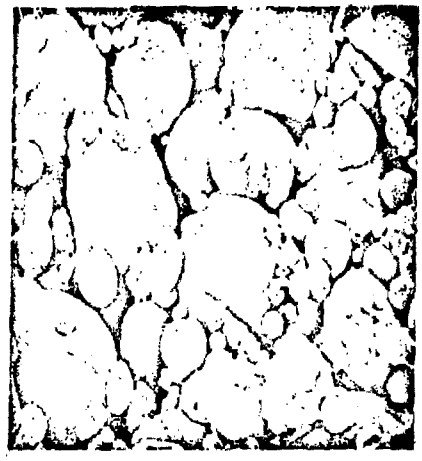

Figure 17(a) Hydrogen sintered lead powders (60 min, 270°C) (SEM, 3000X).

Figure 17(b) Hydrogen sintered lead powders (60 min, 280°C) (SEM, 3000X).

Figure 17(c) Hydrogen sintered lead powders (60 min, 290°C)(SEM, 3000X).

Figure 17(d) Hydrogen sintered lead powders (60 min, 300°C)(SEM, 3000X).

Figure 18(a) Hydrogen sintered lead powders (60 min, 290°C)(SEM, 3000X).

Figure 18(b) Hydrogen sintered lead powders (120min, 290°C)(SEM, 3000X).

Figure 18(c) Hydrogen sintered lead powders (240 min, 290°C) (SEM, 3000X).

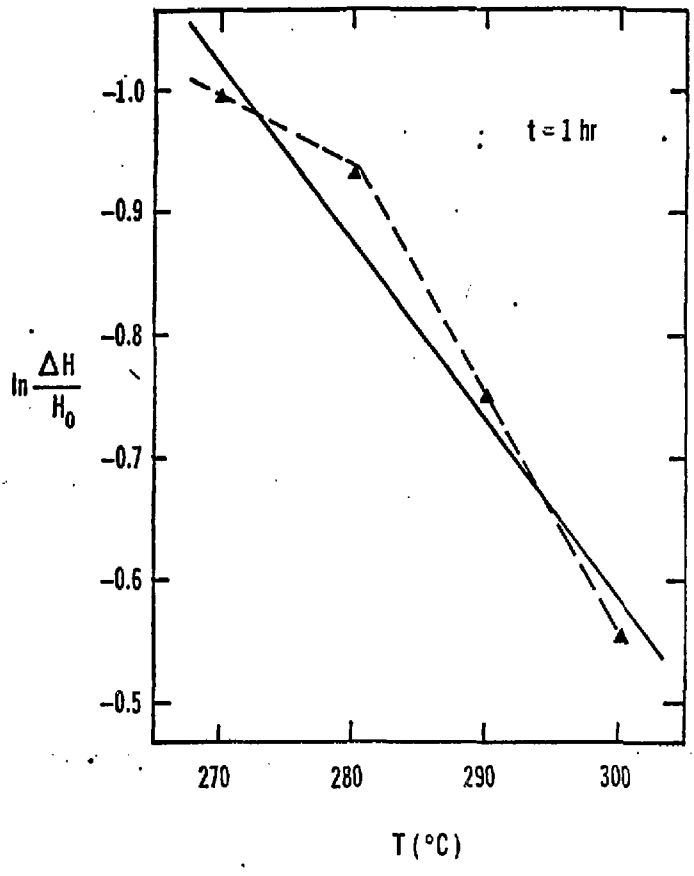

Figure 19 Variation of hardness with temperature for lead compacts sintered in hydrogen (t = 60 min).

to take place between the temperatures of 280° and 290°C as seen from the microstructures of Figures 17b and 17c, respectively. Scanning electron micrographs of lead pellets sintered at 290°C in hydrogen for various times are shown in Figure 18. Figures 18a through 18c represent sintering times of 1, 2, and 4 hr, respectively. Neck growth is apparent and pore closure is evident at the longer sintering times. Figure 19 is a plot of change in hardness as a function of sintering temperature, see Appendix 2. The solid line represents the best fit for all data points and the dashed lines represent a case in which a change in mechanism is assumed between the sintering temperatures of 280° and 290°C.

DISCUSSION

The most apparent indication of the occurence of sintering is the growth of the neck region between particles within a powder compact. Initial formation and growth of the necks between particles of lead sintered in vacuum is evident from Figures 10 through 12. As an example, when the sequence of Figure 12 is compared with the micrographs of the as-pressed samples (Figure 10), an increase in the neck dimension is seen even at t = 30 min (Figure 12a). These observations, coupled with the absence of shrinkage, indicate surface-transport as the rate controlling mass-transport mechanism in the sintering of lead powders in vacuum. As previously stated, the difference between the magnification of Figures 11 and 12 makes direct comparison of the two difficult. However, careful examination shows an increase in the growth rate of the necks between particles as the sintering temperature is increased from 250° to 280°C. Regardless of mechanism, this is to be expected since the value of B in Kuczynski's equation is an exponential function of the temperature through the diffusivity term.

Direct correlation of the slopes of the lines obtained for the change of hardness versus isothermal sintering time (Figure 13) with the sintering mechanism has not been analytically demonstrated. However, it would be expected that as the average neck size increases the resistance to penetration by a hardness indentor would also increase. The results shown in Figure 13 support these expectations. A relationship between hardness and sintering time would also be a function of the sintering mechanism. This is evident from a comparison of the sintering results in hydrogen to those obtained under vacuum, Figure 13.

Since evaluation of the vacuum sintering data supports the conclusion that a surface-transport mechanism is controlling, the exact nature of the

mechanism must now be inferred. Two surface-transport mechanisms can occur: evaporation-condensation and surface diffusion. Since the vapor pressure of lead in the solid state is always lower than 1.3 nPa (10^{-11} torr)[21] evaporation-condensation cannot be a significant mass-transport mechanism. Therefore, it is concluded that surface diffusion is the dominant sintering mechanism of lead powder under vacuum conditions.

For surface diffusion sintering, the value of N obtained from Kuczynski's equation[4,7] is 7. However, recent calculations by Munir, Higgins, and German[11] have shown that this value may range between 6.5 and 8.0 depending upon the initial particle coordination and subsequent neck growth within the powder compact. The values of N obtained for the sintering of lead in vacuum in this work are 5.8 at 250°C, 5.3 at 268°C, and 6.7 at 280°C. Only the value of 6.7, calculated from the data collected at 280°C, lies within the range of values given above. Several possible reasons for the discrepancy between the value of N obtained experimentally and the value obtained theoretically have been considered. They include the effect of multiple mechanism sintering and, since the initial compact density is approximately 68%, the possible isolation of pores within the sintering compact. Moreover, the role of a surface oxide layer can be significant in this case. These considerations will be dealt with below.

If multiple mechanism sintering[12] is in fact occuring the slope of the log $\Delta S/S_0$ versus log t line varies accordingly. Lack of shrinkage during sintering excludes any contribution by bulk-transport mechanisms. Since the evaporation-condensation mechanism has already been shown to be unimportant, the possibility of a multiple mechanistic sintering has been disregarded. The effect of pore isolation on the data collected is a consideration which may not be easy to rule out. At densities approaching 70% of theoretical, such as the initial densities of the powders used in this work, the effect of pore isolation of the surface area measurements begins to be significant[20].

Pore isolation results in a surface area reduction which is larger than that generated by the growth of the neck areas. If pore isolation is taking place, the calculated value for the mechanism exponent N will be smaller than the expected value for the mechanism at hand. As stated above the values of N obtained in this work range between 5.3 and 6.7 and are considerably lower at one end of the spectrum than the expected value of 7 for surface diffusion. These values indicate that the effect of pore isolation may be significant on the surface area data collected.

If isolation of pores is occuring the erroneous data obtained for surface area reduction will also contribute to errors in the calculated activation energy of the process. Under condition of pore isolation the calculated activation energies will be higher than otherwise anticipated. A simple empirical formula[22] relating activation energies of volume, grain boundary, and surface diffusion shows that $Q_{VD}/Q_{GBD}/Q_{SD}$ is of the order of 4/2/1 for most metals. The literature value for the activation energy of the volume self-diffusion in polycrystalline lead is 120 kJ/mol (27.9 Kcal/mol)[22]. This corresponds to a surface diffusion activation energy of 29 kJ/mol (7 Kcal/mol). The experimentally obtained value for the activation energy of vacuum sintered lead is 170 kJ/mol (40.7 Kcal/mol) or roughly six times the value derived when surface diffusion is considered to be the operative mechanism. Therefore the effect of pore isolation is again indicated as possibly accounting for this discrepancy. At the present time no method of correcting data for effects of pore isolation exists.

A more important consideration, perhaps, is the influence of a surface oxide layer on the kinetics of sintering lead powders. Since Kuczynski's equation was derived for a one component system the effect of a second phase, e.g. an oxide layer, is not accounted for. If an oxide layer exists then the surface diffusion process may occur by two possible methods (Figure 20). One possible way is for the lead atom to diffuse through the oxide layer and then

diffuse to the neck region on the oxide surface (path b in Figure 20), and the other is for the lead atom to diffuse along the lead-lead oxide interface to the neck region (path a in Figure 20). For the first process to occur the diffusion of the lead through the lead oxide layer must be very rapid with respect to the overall process. If one assumes an oxide layer thickness of 100 Å the time for diffusion, as calculated by $t = x^2/D_{VD}$, where D_{VD} is the diffusivity for volume diffusion, and t is the time necessary to diffuse a distance x, one obtains, at 300°C, a value of t which is of the order of 0.5 μsec, see Appendix 3. A corresponding value for a 1000 Å oxide layer is of the order of 50 μsec. These values are exceedingly small in comparison to the shortest sintering time monitored (1 ksec). Thus this process cannot be ruled out strictly on the basis of kinetics. The value for the volume diffusion activation energy of lead through polycrystalline lead oxide is 280 kJ/mol (66 Kcal/mol)[22]. The value estimated for grain boundary diffusion is then ∿140 kJ/mol (∿33 Kcal/mol) which is close to the value obtained in this work. It should be noted that lead diffusing through polycrystalline lead oxide is not an accurate model for the diffusion of lead along a lead-lead oxide interface and a discrepancy between values of the respective activation energies would be expected. Nevertheless, the agreement between the calculated and measured activation energies suggests that the mass-transport path may be at the lead-lead oxide interface.

Sintering data for pellets in a hydrogen atmosphere demonstrated the effect of the surface oxide. The activation energy obtained from these data was 130 kJ/mol (30 Kcal/mol) which is roughly the value for the activation energy of creep in lead[23]. Since the calculated value of N of about 2 also indicates a viscous flow mechanism, it is concluded that lead sinters by this mode under hydrogen atmosphere and at temperatures in the range of 76 to 92% of the melting point.

One final aspect should be noted concerning the data presented in

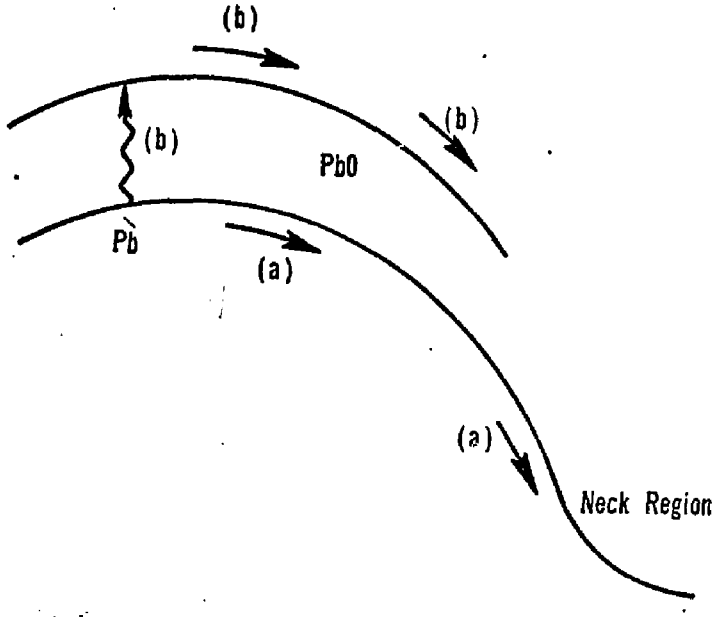

Figure 20 Proposed models for neck growth between lead particles containing a surface oxide layer.

Figure 17. A dramatic change in the microstructure of the sintered pellets occurs between 280° and 290°C. With this in mind the hardness versus sintering temperature data (Figure 19) was interpreted as if there were two mechanisms involved (dashed lines). Although somewhat tenuous, it is possible to assume that a change in mechanism has occured between 280° and 290°C.

The apparent change in mechanism in the sintering of lead powders in a hydrogen atmosphere is believed not to be related to a possible oxide reduction or evaporation process. The free energy of the reaction

$$PbO\ (s) + H_2\ (g,\ 1\ atm) = Pb\ (s) + H_2O\ (g) \qquad (21)$$

is negative (ranging from -50 kJ/mol to -54 kJ/mol, -12 Kcal/mol to -13 Kcal/mol)[17] over the experimental temperature range, see Appendix 3. Thus the reduction of the oxide is thermodynamically possible at all of the sintering temperatures. Furthermore, since the vapor pressure of PbO is exceedingly low at these temperatures, (1.3 nPa to 1.3 pPa, 10^{-11}torr to 10^{-14} torr)[24], it is not likely that evaporation of this oxide from isolated pore surfaces can contribute to the observed shift in sintering behavior, see Appendix 3.

CONCLUSIONS

The results of sintering of 10 - 20 μm sized lead powders in vacuum (130 mPa, 10^{-7} torr) indicate that a surface transport mechanism is rate controlling. Due to the low vapor pressure of lead in the solid state it is concluded that a surface diffusion process is the operative mechanism. From measurements of surface area reduction values of N for this process were found to range from 5.3 to 6.7 for sintering temperatures between 250° and 280°C. Comparison of N to the assumed values show a significant deviation. These discrepancies have been explained in terms of pore isolation for the high green density powders.

The activation energy calculated for sintering of lead powder in vacuum is 170 kJ/mol (40.7 Kcal/mol). This value is nearly six times that calculated for surface diffusion of lead, 29 kJ/mol (7 Kcal/mol). The effect of a surface oxide layer is proposed as a cause for this difference. Comparison of pellets sintered in high vacuum to those sintered in a hydrogen atmosphere supports the conclusion that the oxide is influencing the sintering kinetics. Several models are proposed that allow a quasi-surface diffusion mechanism to occur. Interfacial diffusion along the lead-lead oxide surface seems plausible. A comparison of the estimated activation energy for this proposed model and the activation energy obtained in this work shows good agreement.

In hydrogen atmosphere lead pellets sinter by a bulk-transport mechanism. The calculated activation energy for sintering under these conditions was calculated to be 130 kJ/mol (30 Kcal/mol). This value as well as that of the mechanism exponent N, indicate that the sintering process is controlled by a viscous flow mechanism occuring by grain boundary sliding.

BIBLIOGRPHY

1. Sauerwald, F., Kolloid Z., 44, 104 (1943)

2. Thummler, F., and W. Thomma, Met. Rev., 12, 69 (1967)

3. Frenkel, J., J. Physics (U.S.S.R.), 9, 385 (1945)

4. Kuczynski, G.C., Trans A.I.M.E., 185, 169 (1949)

5. Kuczynski, G.C., J. Appl. Phys., 21, 632 (1950)

6. Herring, C., J. Appl. Phys., 21, 301 (1950)

7. Jellinek, H.H.G., and S.H. Ibrahim J. Colloid Interface Sci., 25, 245 (1967)

8. German, R.M., and Z.A. Munir "Kinetic Model For Reduction In Surface Area During Initial Stage Sintering", Sintering and Catalysis, Ed. by G.C. Kuczynski, Plenum Press, New York, N.Y. (1975)

9. German, R.M., and Z.A. Munir Met Trans, 6B, 289 (1975)

10. German, R.M., and Z.A. Munir Met Trans, 6A, 2229 (1975)

11. Munir, Z.A., P.K. Higgins, and R.M. German Fourth Int. Conference On Sintering, Dubrovnik, Yugoslavia, (Sept. 5-10, 1977)

12. German, R.M. and Z.A. Munir Inter. J. Powder Met. and Powder Tech., 12, 37 (1976)

13. Rhines, F.N., R.T. DeHoff, and R.A. Rummel Agglomeration, Ed. by W.A. Knepper, Interscience, New York, N.Y. (1962) p. 351

14. German, R.M., R.W. Mar, and J.C. Hastings Amer. Cer. Soc. Bull., 54, 178 (1975)

15. German, R.M., and Z.A. Munir J. Amer. Cer. Soc., 59, 379 (1976)

16. Kingery, W.D., Introduction to Ceramics, John Wiley and Sons, New York, N.Y. (1960)

17. Handbook of Chemistry and Physics, 54th Edition, Chemical Rubber Co. Press, Cleveland, Ohio (1973-74)

18. Smith, R.C., Journal of the Ceramic Soc., 119, 2088 (1921)

19. Smart, R.F., and E.C. Ellwood Nature, 181, 833 (1958)

20. Model 2100 ORR Surface-Area Pore-Volume Analyzer Instruction Manual, Micrometrics Instrument Corp. Atlanta, Ga., (1969)

21. Honig, R.E., RCA Review, 23, (#4), 567 (1962)

22. Askill, J., Tracer Diffusion Data For Metals, Alloys, and Simple Oxides, IFI/Plenum Data Corporation, New York, N.Y., (1970)

23. Mukherjee, A.K., J.E. Bird, and J.E. Dorn Amer. Soc. Metals Trans. Quart., 62, 155 (1969)

24. J.A.N.A.F. Thermochemical Tables, Dow Chemical Corp. Thermal Research Lab., Ed. by D.R. Stull and H. Prophet, U.S. Bureau of Mines Report # NSRDS-NB337, Midland, Michigan, (1971)

APPENDICES

APPENDIX 1

a) The B.E.T. method.

b) Representative data sheets for surface area measurements of vacuum sintered lead compacts.

Appendix 1-a: The B.E.T. method.

The rate of condensation of gas molecules onto an adsorbed layer is related to the rate of evaporation from that layer. By summing for an infinite number of layers the following expression is obtained:

$$\frac{P}{V_a (P_s - P)} = \frac{1}{V_m C} + \frac{C-1}{V_m C} (P/P_s) \qquad \text{(A-1)}$$

where V_a is the volume of gas adsorbed at pressure P, V_m is the volume adsorbed when the entire adsorbing surface is covered by a monomolecular layer, P_s is the saturation pressure of the gas, and C is a constant. P_s is actually the vapor pressure at a given temperature of a large quantity of gas condensed into a liquid.

Since Equation A-1 is expressed in a linear form a plot of data for $P/\left[V_a(P_s - P)\right]$ versus P/P_s gives a straight line the slope of which is $(C-1)/V_m C$ and the intercept of which is $1/V_m C$. This allows V_m to be calculated by several measurements. From this information and knowledge of the physical dimensions of single molecules of the adsorbant, the surface area of the adsorbing solid may be calculated.

Final calculation of the surface area is made by use of the expression:

$$\frac{V_a}{W_s} = \frac{273}{760\ W} \left[\frac{V_d}{T_d} (P_1 - P_2) - \left(\frac{V_s}{T_s} + \frac{V_i}{T_i} \right) (P_2 - P_e) - \frac{V_s}{T_s} \alpha (P_2^2 - P_e^2) \right] \qquad \text{(A-2)}$$

where V_s, V_i, and V_a are, respectively, the volume of the free space about the sample, the volume of interconnecting tubing, and the volume of the gas removed by adsorption, W_s is the sample weight, P_e is the equilibrium pressure, α is the perfect gas law correction, V_d and T_d are the volume and

temperature of the distributing manifold, V_i and T_i are the volume and temperature measured at an intermediate time, P_1 and P_2 are measurements of the pressure at times t_1 and t_2 , and V_s and T_s are the volume and temperature of the specimen during the test.

A plot of V_a/W_s versus P_2/P_s, where P_s is the saturation pressure, yields an adsoption isotherm. This allows V_m to be calculated by back substitution of values into Equation A-1.

Once a value for V_m has been established the specific surface area is calculated by:

$$S_w = \frac{S \times 10^{-20} \times 6.023 \times 10^{23}}{22.414 \times 10^3 \text{ (slope + intercept)}} \qquad \text{(A-3)}$$

where the slope and intercept are those of Equation A-1 and S is the area covered by one molecule of the adsorbant in Å^2.

For the measurements made on the lead compacts of this study, krypton gas was used as an adsorbant. For these measurements

$$S = 21.0\ \text{Å}^2 \text{ at } 77^\circ\text{K}$$

$$\alpha = 3 \times 10^{-5}\ (\text{mmHg})^{-1}$$

$$V_d = 24.14 \text{ ml}$$

Thus the final expression obtained is

$$S_w = \frac{5.643}{\text{(slope + intercept)}}\ m^2/gm \qquad \text{(A-4)}$$

Use of the above expression result in an instantaneous surface area and when compared with an initial value, S_o, represents the change in surface area of the compact.

Appendix 1-b: Representative data sheets for surface area measurements of vacuum sintered lead compacts.

SURFACE AREA ANALYSIS

15 DEC 76

LEAD PELLETS 250 1 HOUR PE0761228

V1 =	37.7940	H1 =	500.000	XV =	129.000	PS =	2.499
V2 =	32.2615	H2 =	108.110		KRYPTON	ALPHA =	3.000E-05
VS =	5.5325	TS =	77.370	VC =	24.140	S =	21.0

#	X	P1	P2	VA	P2/PS	X/V(1-X)
1		.4132	.0014	.0021	.0006	.2702
2		.3492	.0030	.0039	.0012	.3154
3		.2755	.0046	.0053	.0018	.3502
4		.4176	.0069	.0073	.0028	.3783
5		.3537	.0084	.0091	.0034	.3726
6	X	.3001	.0247	.0177	.0099	.5652
7	X	.4793	.1438	.0263	.0575	2.3201
8		.5050	.1759	.0274	.0704	2.7633
9		.4539	.2028	.0282	.0811	3.1336
10		.4148	.2240	.0288	.0896	3.4228
11		.3953	.2408	.0292	.0962	3.6528
12		.4536	.2636	.0297	.1056	3.9691
13		.4240	.2816	.0301	.1127	4.2146
14		.5021	.3063	.0307	.1226	4.5540
15		.4718	.3254	.0311	.1302	4.8187
16		.4491	.3397	.0314	.1359	5.0164

BET EQUATION CONSTANTS :
INTERCEPT = 3.4284E-01
SLOPE = 3.4370E+01

SURFACE AREA = .160 SQ. METERS/GM
STANDARD DEVIATION = .00138

X	P_1	P_2	P_s	D	E	F	G	H	J	V_a/W_s	V	x	y
	.4132	.0014											
	.3492	.0030											
	.2755	.0046											
	.4176	.0069											
	.3537	.0084											
X	.3001	.0247											
X	.4793	.1438											
	.5050	.1759											
	.4539	.2028											
	.4148	.2240											
	.3953	.2408											
	.4536	.2636											
	.4240	.2816											
	.5021	.3063											
	.4718	.3254											
	.4491	.3397											

LEAD PELLETS 250 1 HOUR RE0761228 15 DEC 76

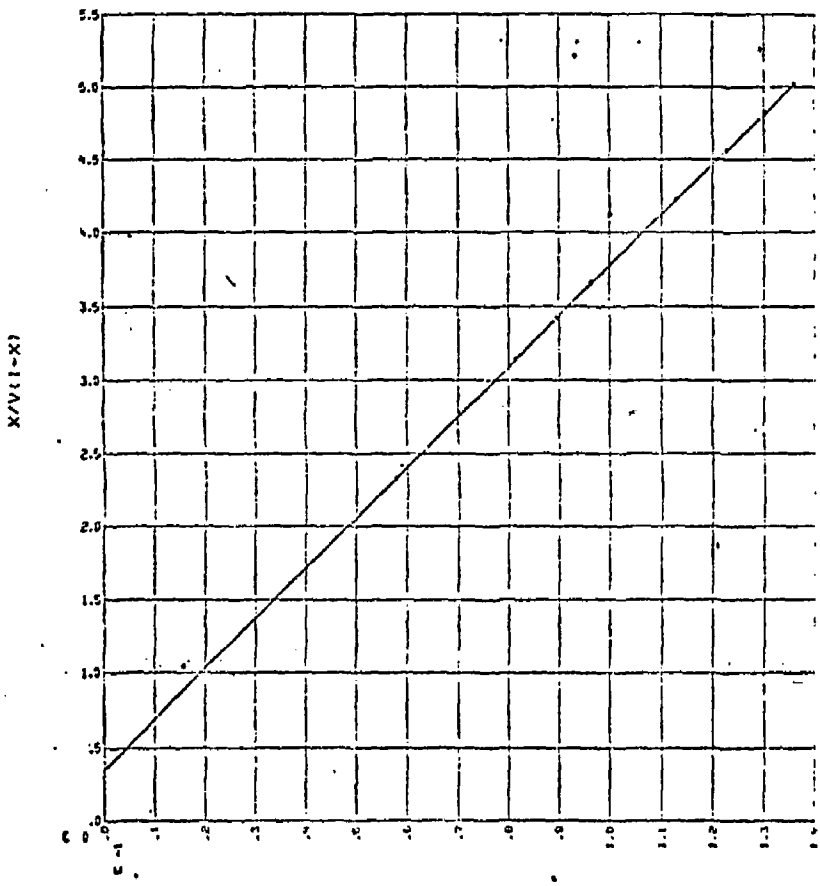

SURFACE AREA ANALYSIS 15 DEC 76

LEAD PELLETS 250 120 MINUTES PE0761228

W1 =	37.5121	H1 =	500.100	XV =	129.000	PS =	2.499
W2 =	29.7405	H2 =	106.650		KRYPTON	ALPHA =	3.000E-05
WS =	7.7716	TS =	77.370	VI =	24.140	S =	21.0

#	X	P1	P2	VA	P2/PS	X/V(1-X)
1	X	.5217	.0120	.0116	.0048	.4166
2	X	.5769	.0743	.0223	.0297	1.3728
3		.6257	.1031	.0233	.0413	1.8053
4		.5444	.1315	.0250	.0526	2.2257
5		.5672	.1632	.0260	.0652	2.6375
6		.5042	.1905	.0268	.0762	3.0824
7		.5902	.2247	.0276	.0899	3.5731
8		.5360	.2527	.0283	.1011	3.9745
9		.4920	.2747	.0288	.1099	4.2383
10		.6867	.3143	.0296	.1258	4.8569
11		.6292	.3452	.0302	.1381	5.3005

BET EQUATION CONSTANTS :
INTERCEPT = 3.4101E-01
SLOPE = 3.5919E+01

SURFACE AREA = .156 SQ. METERS/GM
STANDARD DEVIATION = .00283

$\frac{}{W_0 \ T_0}$ = _____ S_0 = $\frac{}{(\text{slope} + \text{intercept})}$ = _____ m^2/gm

				D	E	F	G	H	J	V_0/W_1	V	x	y
X	P_1	P_2	P_s	P_1-P_2	P_2-P_s	$P_2^2-P_s^2$	A×D	B×E	C×F	G-H-J	$\Sigma \frac{V_0}{W_1}$	P_2/P_s	$\frac{x}{V(1-x)}$
X	.5217	.0120											
X	.5769	.0743											
	.6257	.1031											
	.5444	.1315											
	.5672	.1632											
	.5042	.1905											
	.5902	.2247											
	.5360	.2527											
	.4920	.2747											
	.6867	.3143											
	.6292	.3452											

LEAD PELLETS 250 120 MINUTES REQ76122B 15 DEC 76

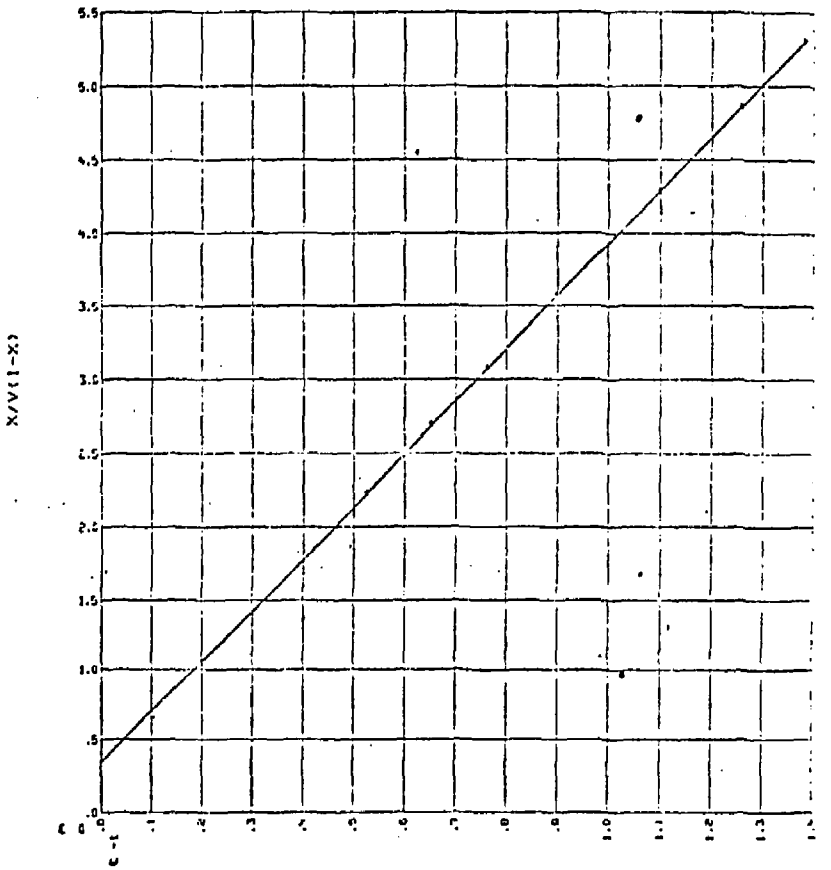

[illegible] [illegible] [illegible] — 27 JAN 77 (?)

[illegible] [illegible] CASE I II [illegible]

[illegible] =	2?.6??	[illegible] =	5??.2??	[illegible] =	1?9.000	[illegible] =	[illegible]
[illegible] =	??.??47	[illegible] =	1??.???		[illegible]	[illegible] =	?.????-0?
[illegible] =	?.?1?1	[illegible] =	77.200	[illegible] =	??.1??	[illegible] =	?1.0

X	P1	P2	[illegible]	[illegible]	X/(1-X) (?)
1 X	.5196	.0234 (?)	.01??	.0???	.0155 (?)
2 X	.6007	.1336	.00??	.0???	?.????
3	.5779 (?)	.1713	.0045 (?)	.0?-7	?.4?76
4	.5287 (?)	.2041 (?)	.0305	.0?1?	?.????
5	.4700	.2306 (?)	.031?	.0???	3.3?71 (?)
6	.4328 (?)	.2515	.0317 (?)	.1009 (?)	3.5???
7	.6017	.2790 (?)	.0206	.1159 (?)	4.0?64
8	.5528 (?)	.3184 (?)	.033?	.1277 (?)	4.4151 (?)
9	.5167	.3400 (?)	.032?	.1266	4.7559 (?)

[illegible] CONSTANTS :
INTERCEPT (?) = 2.67?7E-01
SLOPE (?) = 2.0451E+01

[illegible] AREA (?) = .175 SQ. METERS/GM (?)
STANDARD DEVIATION (?) = .00191

$S = \frac{.03593\ V_1 a}{W_s\ T_s}$ = ______________ $S_x = \frac{.0?0?? S}{(\text{slope} + \text{intercept})}$ = ______________ m^2/gm

				D	E	F	G	H	J	V_s/W_s	V	x	y
X	P_1	P_2	P_e	$P_1 - P_2$	$P_2 - P_e$	$P_2^2 - P_e^2$	A+D	B+E	C+F	G-H-J	$\Sigma \frac{V_s}{W_s}$	P_2/P_0	$\frac{x}{V(1-x)}$
✓	.5196	.0234											
X	.6007	.1336											
	.5779 (?)	.1713											
	.5287	.2041											
	.4700	.2306											
	.4328	.2515											
	.6017	.2790 (?)											
	.5528 (?)	.3184											
	.5167	.3400 (?)											

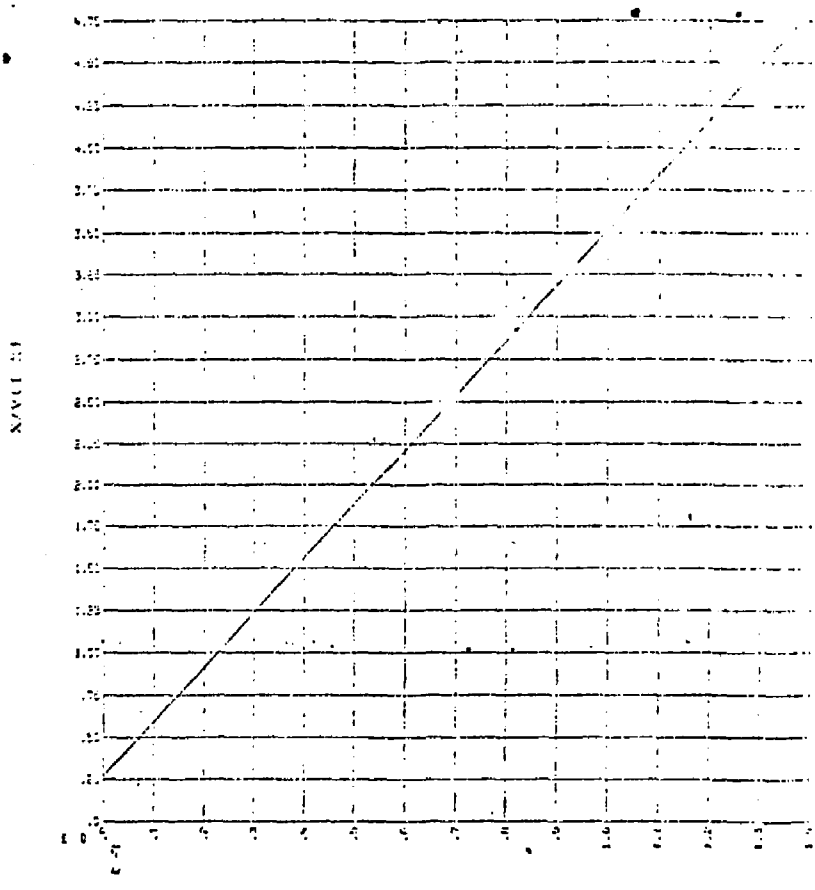

RELATIVE PRESSURE (P2/PS)

SURFACE AREA ANALYSIS — 2[illegible] JAN 77

[illegible] 5[illegible]77C46

W1 =	27.9[illegible]	H1 =	5[illegible]1.2[illegible]	XV =	1[illegible]3.[illegible]	[illegible] =	2.[illegible]
W2 =	2[illegible].[illegible]	H2 =	1[illegible].[illegible]20		[illegible]	[illegible] =	2.[illegible]L-0[illegible]
W[illegible] =	5.[illegible]	T[illegible] =	77.[illegible]	W[illegible] =	[illegible]	[illegible] =	[illegible]1.[illegible]

# X	P1	P2	[illegible]	[illegible]	[illegible]
1 X	.5[illegible]	.0[illegible]	.0172	.0100	.[illegible]
2 X	.[illegible]106	.1[illegible]	.0[illegible]79	.0[illegible]	[illegible]
3	.[illegible]	.[illegible]	.0[illegible]1	.0[illegible]	2.[illegible]
4	.5[illegible]	.[illegible]71	.0[illegible]	.10[illegible]	[illegible]
5	.51[illegible]	.[illegible]	.0[illegible]	.11[illegible]	[illegible]
6	.4[illegible]7	.31[illegible]	.0[illegible]11	.1[illegible]	[illegible]
7	.[illegible]577	.3[illegible]	.0[illegible]	.1[illegible]	[illegible].9[illegible]
8	.[illegible]	.[illegible]	.0[illegible]1[illegible]	.1[illegible]	[illegible]

FIT EQUATION CONSTANTS :
INTERCEPT = 0.2[illegible]-01
SLOPE = 0.[illegible]+01

SURFACE AREA = .1[illegible]2 SQ. METERS/GM
STANDARD DEVIATION = .00[illegible]6

(slope + intercept) ______ m²/gm

				D	E	F	G	H	J	V_a/W_s	V	x	Y
X	P_1	P_2	P_4	P_1-P_2	P_2-P_4	$P_2^2-P_4^2$	A×D	B×E	C×F	G-H-J	$\Sigma \frac{V_a}{W_s}$	P_2/P_o	$\frac{x}{V(1-x)}$
✓	.5993	.0377											
✓	.2106	.1284											
	.6251	.2314											
	.5645	.2671											
	.5182	.2941											
	.4837	.3162											
	.4577	.3374											
	.4355	.3446											

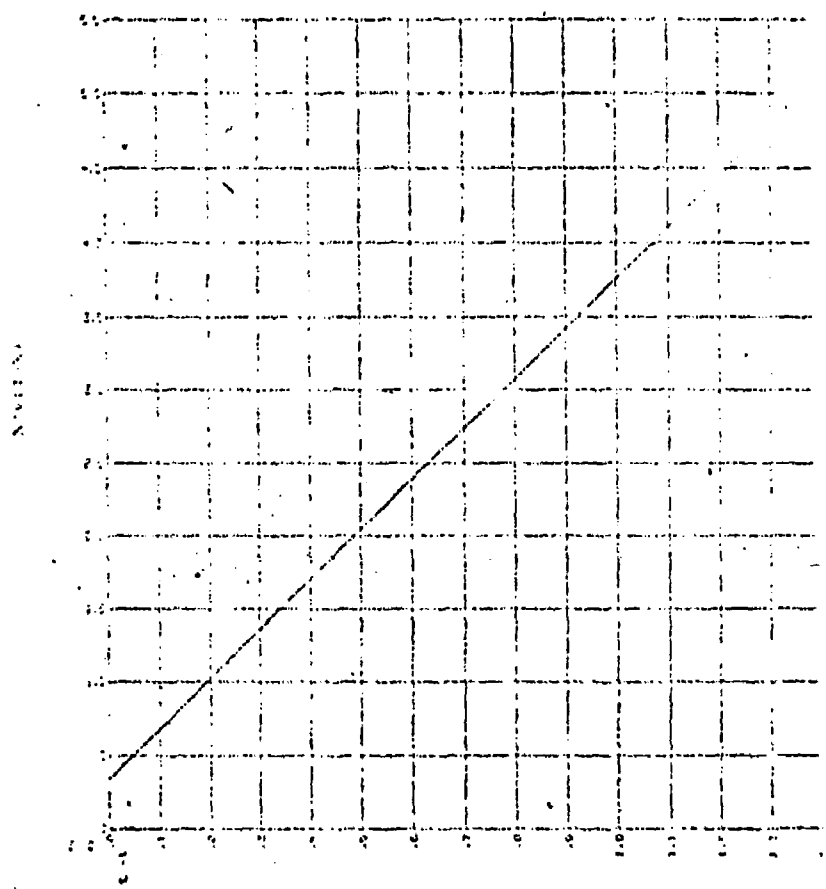

RELATIVE PRESSURE (P2/P1)

SURFACE AREA ANALYSIS 16 DEC 76

LEAD PELLETS AS IS. PEC761228

V1 =	38.037C	H1 =	500.000	XV =	129.000	PS =	2.472
V2 =	29.4581	H2 =	106.780		KRYPTON	ALPHA =	3.000E-05
VS =	8.5739	TS =	77.320	VD =	24.140	S =	21.0

# X	P1	P2	VA	P2/PS	X/V(1-X)
1 X	.6036	.0479	.0110	.0194	1.7940
2 X	.5689	.1464	.0136	.0592	3.3779
3	.6722	.1670	.0201	.0676	3.6198
4	.7165	.1996	.0215	.0767	3.9624
5	.8079	.2164	.0231	.0875	4.1482
6	.8295	.2444	.0247	.0989	4.4396
7	.8100	.2721	.0261	.1101	4.7306
8	.7266	.2959	.0273	.1197	4.9855
9	.6594	.3157	.0282	.1277	5.1982
10	.6057	.3327	.0289	.1346	5.3393
11	.5633	.3465	.0294	.1402	5.5444

BET EQUATION CONSTANTS :
INTERCEPT = 1.8184E+00
SLOPE = 2.6516E+01

SURFACE AREA = .199 SQ. METERS/GM
STANDARD DEVIATION = .00772

				. D	E	F	G	H	J	V_a/V_s	V	x	y
X	P_1	P_2	P_a	P_1-P_2	P_2-P_a	$P_2^2-P_a^2$	A÷D	B÷E	C÷F	G-H-J	$\leq \frac{V_a}{W_s}$	P_2/P_1	$\frac{x}{V(1-x)}$
Y	.6036	.0479											
X	.5689	.1464											
	.6722	.1670											
	.7165	.1996											
	.8079	.2164											
	.8295	.2444											
	.8100	.2721											
	.7266	.2959											
	.6594	.3157											
	.6057	.3327											
	.5633	.3465											

LEAD PELLETS AS IS REQ 761208 17 DEC 76

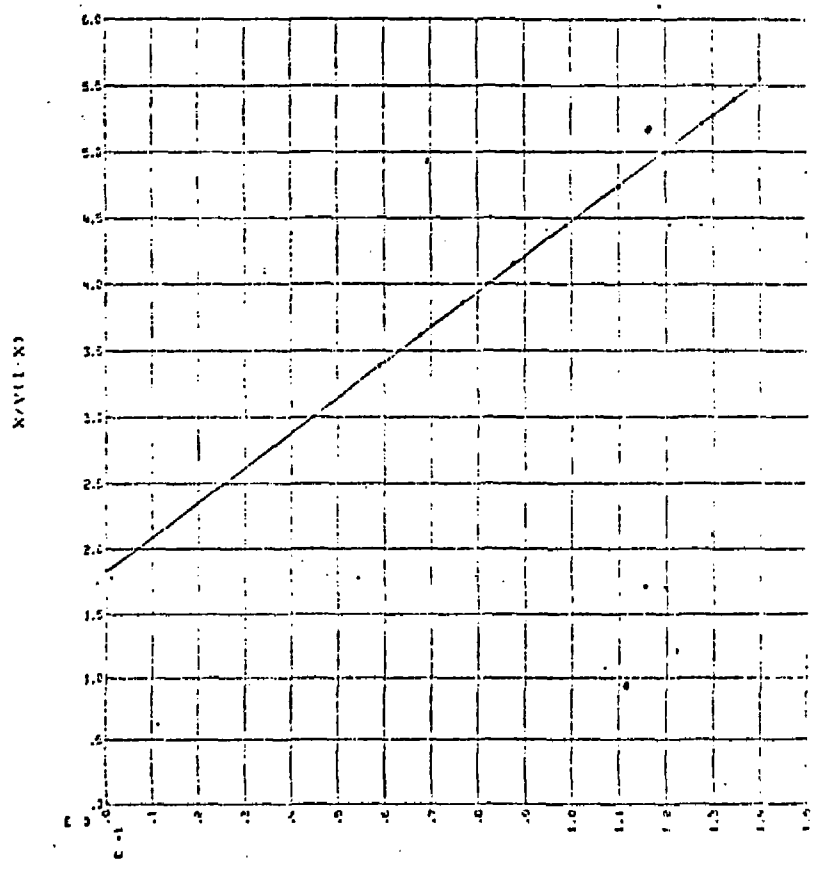

APPENDIX 2

a) Preliminary data for 99.9% pure lead sintered in vacuum.

b) Preliminary hardness data for vacuum sintered lead pellets.

c) Instantaneous surface area data for vacuum sintered lead pellets.

d) Data for lead pellets sintered in a hydrogen atmosphere.

e) Preliminary data for the hardness of hydrogen sintered lead pellets.

Appendix 2-a: Preliminary data for 99.9% pure lead sintered in vacuum.

Time (hr)	Sample	Mass (gm)	Volume (cm^3)	ρ (gm/cm^3)	%ρ	L_1 (cm)	L_2 (cm)
T = 250°C							
1/2	1	1.93	0.251	7.69	67.7	0.759	0.749
	2	1.84	0.236	7.80	68.6	0.704	0.704
	3	1.94	0.253	7.67	67.5	0.759	0.757
	4	1.92	0.243	7.90	69.6	0.726	0.726
1	1	1.92	0.248	7.74	68.2	0.741	0.740
	2	1.82	0.233	7.81	68.8	0.698	0.696
	3	1.95	0.254	7.28	64.1	0.760	0.760
	4	1.92	0.248	7.74	68.2	0.743	0.740
2	1	1.92	0.248	7.74	68.2	0.741	0.740
	2	1.93	0.250	7.72	68.0	0.748	0.748
	3	1.86	0.240	7.77	68.4	0.719	0.716
	4	1.85	0.240	7.73	68.0	0.720	0.718
5	1	1.96	0.253	7.75	68.2	0.740	0.740
	2	1.89	0.244	7.75	68.1	0.730	0.730
	3	1.85	0.239	7.74	68.1	0.715	0.715
	4	1.87	0.243	7.69	67.7	0.726	0.726
T = 268°C							
1/2	1	1.94	0.250	7.76	68.3	0.749	0.748
	2	1.89	0.246	7.68	67.6	0.739	0.734
	3	1.87	0.241	7.78	68.5	0.731	0.720
	4	1.85	0.239	7.74	68.1	0.720	0.714
1	1	1.90	0.245	7.75	68.3	0.736	0.733
	2	1.93	0.252	7.68	67.6	0.755	0.754
	3	1.88	0.245	7.67	67.5	0.732	0.732
	4	1.89	0.247	7.67	67.5	0.740	0.739
2	1	1.86	0.243	7.65	67.4	0.724	0.724
	2	1.92	0.251	7.65	67.3	0.749	0.749
	3	1.91	0.251	7.65	67.0	0.748	0.747
	4	1.82	0.238	7.67	67.5	0.712	0.711
5	1	1.89	0.247	7.67	67.5	0.744	0.732
	2	1.88	0.244	7.70	67.8	0.732	0.728
	3	1.90	0.251	7.57	66.6	0.750	0.749
	4	1.95	0.256	7.34	67.2	0.771	0.766

Time (hr) T = 280°C	Sample	Mass (gm)	Volume (cm^3)	ρ (gm/cm^3)	%ρ	L_1 (cm)	L_2 (cm)
1/2	1	1.89	0.246	7.68	67.6	0.741	0.735
	2	1.98	0.256	7.75	68.3	0.773	0.765
	3	1.89	0.245	7.71	67.9	0.738	0.732
	4	1.86	0.240	7.77	68.4	0.726	0.718
1	1	1.89	0.244	7.75	68.2	0.738	0.729
	2	1.99	0.259	7.70	67.8	0.779	0.772
	3	1.87	0.243	7.72	67.9	0.729	0.725
	4	1.86	0.242	7.71	67.8	0.731	0.724
2	1	1.91	0.247	7.75	68.2	0.742	0.738
	2	1.93	0.251	7.69	68.3	0.733	0.726
	3	1.88	0.243	7.76	68.3	0.733	0.726
	4	1.90	0.247	7.69	67.7	0.737	0.737
5	1	1.90	0.248	7.68	67.6	0.749	0.742
	2	1.88	0.246	7.64	67.3	0.736	0.734
	3	1.89	0.247	7.65	67.4	0.740	0.737
	4	1.86	0.244	7.64	67.3	0.732	0.728
Unsintered							
	1	1.85	0.242	7.64	67.3	0.723	
	2	1.88	0.246	7.64	67.3	0.736	
	3	1.88	0.248	7.60	66.9	0.742	
	4	1.85	0.245	7.57	66.6	0.733	
	5	1.97	0.256	7.69	67.7	0.756	
	6	1.88	0.244	7.70	67.8	0.729	
	7	1.95	0.258	7.58	66.7	0.772	
	8	1.95	0.256	7.64	67.2	0.765	

Appendix 2-b: Preliminary hardness data for vacuum sintered lead pellets.

Time (hr)	Filar Reading (avg)	Vicker's Hardness
T = 250°C		
As Is	4.94	28.5
1/2	4.51	29.1
1	4.25	29.5
2	4.10	29.9
5	3.55	30.9
T = 268°C		
As Is	3.98	30.0
1/2	3.56	30.9
1	3.25	31.5
2	2.98	32.0
5	2.62	32.6
T = 280°C		
As Is	3.98	30.0
1/2	3.45	31.0
1	3.15	31.7
2	2.87	32.2
5	2.56	32.8

Appendix 2-c: Instantaneous surface area data for vacuum sintered lead pellets.

Time (hr)	Surface Area (m^2/gm)	$\Delta S/S_o$
T = 250°C		
1/2	0.165	0.050
1	0.182	0.086
2	0.174	0.126
5	0.169	0.151
T = 268°C		
1/2	0.179	0.100
1	0.172	0.136
2	0.164	0.176
5	0.152	0.236
T = 280°C		
1/2	0.172	0.136
1	0.163	0.181
2	0.156	0.216
5	0.142	0.286

For calculation of the activation energy of the process the following data was used.

Temperature (°C)	Inverse Temperature ($^oK^{-1}$)	$\Delta S/S_o$
250	1.911×10^{-3}	0.144
268	1.848×10^{-3}	0.170
280	1.808×10^{-3}	0.216

Appendix 2-d: Data for lead pellets sintered in a hydrogen atmosphere.

Temperature (°C)	Time (hr)	Initial Density (gm/cm^3)	Final Density (gm/cm^3)
270	1	7.856	7.935
280	1	7.846	7.978
290	1	7.798	8.071
290	2	7.747	9.124
290	4	7.745	9.353
300	1	7.895	8.973

Appendix 2-e: Preliminary data for the hardness of hydrogen sintered lead pellets.

Temperature (°C)	Time (hr)	Filar Units	Vicker's Hardness
270	1	5.12	15.3
280	1	4.94	15.5
290	1	4.79	16.5
290	2	4.54	18.4
290	4	4.29	20.6
300	1	4.65	17.5

APPENDIX.3

a) Calculation of the diffusion time for lead through lead oxide.

b) Calculation of the vapor pressure of lead oxide for the temperature range between 250^{0} and 290^{0}C.

c) Calculation of ΔG for the reaction

$$PbO\ (s) + H_2\ (g) \rightleftarrows Pb\ (s) + H_2O\ (g)$$

Appendix 3-a: Calculation of the diffusion time for lead through lead-oxide

$$t = x^2/D_{VD}$$

$x_1 = 100$ Å

$x_2 = 1000$ Å

$D_o = 10^5$ cm^2/sec*

$Q = 27.9$ Kcal/mol*

$R = 1.98$ cal/mol

$T = 300^oC = 573.15^oK$

$$D_{VD} = D_o \exp(-Q/RT)$$

$$= 10^5 \exp(-27900/1.98 \times 573.15) \text{ cm}^2/\text{sec}$$

$$= 2.103 \times 10^{-6} \text{ cm}^2/\text{sec}$$

For $x = x_1$

$$t = (10^{-6})^2/ 2.103 \times 10^{-6} \text{ sec}$$

$$= 5 \times 10^{-7} \text{ sec} = 0.5 \mu\text{sec}$$

For $x = x_2$

$$t = (10^{-5})^2/ 2.103 \times 10^{-6} \text{ sec}$$

$$= 5 \times 10^{-5} \text{ sec} = 50 \mu\text{sec}$$

* Askill, J., Tracer Diffusion Data For Metals, Alloys, and Simple Oxides, IFI/Plenum Data Corporation, New York, N.Y., (1970)

Appendix 3-b: Calculation of the vapor pressure of lead oxide for the temperature range between 250° and 290°C.

From the Handbook of Chemistry and Physics:

$$\log_{10}(v.p.) = -(0.2185\ A/T) + B$$

where v.p. = vapor pressure (torr)

A = heat of vaporization = 52862.2 cal/gm mol

B = 9.502627

T = temperature (absolute)

@ 250°C v.p. = 2.655×10^{-13} torr

260°C = 6.890×10^{-13} torr

270°C = 1.726×10^{-12} torr

280°C = 4.183×10^{-12} torr

290°C = 9.824×10^{-12} torr

Therefore: At temperatures used in this experiment the vapor pressure of lead oxide is always lower than 10^{-11} torr.

Appendix 3-c: Calculation of ΔG for the reaction

$$PbO\ (s) + H_2\ (g) \rightleftarrows Pb\ (s) + H_2O\ (g)$$

From the J.A.N.A.F. Thermochemical Tables

Element	$\Delta H^o_{f\ 298}$ (Kcal/mol)	T (^oK)	$H^o_T - H^o_{298}$ (Kcal/mol)	S^o_T (cal/mol)
Pb	0	400.0	0.664	17.399
		500.0	1.337	18.898
		600.0	2.027	20.157
PbO	-52.410	400.0	1.158	18.928
		500.0	2.368	21.626
		600.0	3.369	23.940
H_2	0	400.0	0.707	33.247
		500.0	1.406	34.806
		600.0	2.106	36.082
H_2O	-57.798	400.0	0.825	47.484
		500.0	1.634	49.334
		600.0	2.509	50.891

$G = H - TS$

$\Delta G = G(prod) - G\ (react)$

$\Delta H^o_{298} = H^o_{298}(prod) - H^o_{298}(react)$

$= -57.798 + 52.410$ Kcal/mol

$= -5.388$ Kcal/mol

$$G = \int_{Pb} C_p dT + \int_{H_2O} C_p dT - \left[\int_{PbO} C_p dT + \int_{H_2} C_p dT\right] + \Delta H^o_{298}$$

$$- T\left[S^o_{Pb} + S^o_{H_2O} - (S^o_{PbO} + S^o_{H_2})\right]$$

@ 400°K $\Delta G = 664 + 825 - 1158 - 707 - 5387.9$
$- 400\ (17.399 + 47.484 - 18.928 - 33.247)$

$= -10.85$ Kcal/mol

@ 500°K $\Delta G = 1337 + 1654 - 2368 - 1406 - 5387.9$
$- 500\ (18.898 + 49.334 - 21.626 - 34.806)$

$= -12.07$ Kcal/mol

@ 600°K $\Delta G = 2027 + 2509 - 2368 - 1406 - 5387.9$
$- 600\ (20.157 + 50.891 - 23.940 - 36.082)$

By a statistical linear regression:

$$\Delta G = (-1.185 \times 10^{-2}\ T) - 6.115 \text{ Kcal/mol}$$

$$R = .9995$$

Therefore:

@ 250°C	$\Delta G = -12.31$ Kcal/mol
260	$= -12.43$
270	$= -12.55$
280	$= -12.67$
290	$= -12.79$
300	$= -12.91$

and the ΔG for the reaction is always highly negative and will be driven to the right for the above temperature range.